

## Design and modeling of energy generated magneto rheological damper

Raju Ahamed\*, Muhammad Mahbubur Rashid<sup>†</sup>, Md Meftahul Ferdous and Hazlina Md. Yusof

Department of Mechatronics Engineering, International Islamic University Malaysia, Kuala Lumpur 53100, Malaysia

(Received October 12, 2015; final revision received December 6, 2015; accepted January 9, 2016)

In this paper an energy generated mono tube MR damper model has been developed for vehicle suspension systems. A 3D model of energy generated MR damper is developed in Solid Works electromagnetic simulator (EMS) where it is analyzed extensively by finite element method. This dynamic simulation clearly illustrates the power generation ability of the damper. Two magnetic fields are induced inside this damper. One is in the outer coil of the power generator and another is in the piston head coils. The complete magnetic isolation between these two fields is accomplished here, which can be seen in the finite element analysis. The induced magnetic flux densities, magnetic field intensities of this damper are analyzed for characterizing the damper's power generation ability. Finally, the proposed MR damper's energy generation ability was studied experimentally.

**Keywords:** magneto rheological damper, MR fluid, power generation, EMS, finite element

### 1. Introduction

The vehicle suspension system offers a comfortable journey for both driver and passengers and at present it is a realistic subject of research because of increasing high-speed machines or other systems. Among the three suspension systems, semi-active suspension system provides improved ride quality which can work in passive condition and when the control system does not work it works similar to active suspension system. Semi-active suspension is the combination of the advantages of active and passive suspension systems and it gives economical benefit and better performance with small power supply (Karnopp *et al.*, 1974). MR fluid based dampers are very hopeful for semi-active or adaptive control system which is filled with one kind of smart material known as MR fluid (Lai and Liao, 2002; Shen *et al.*, 2006; Gattulli *et al.*, 2008). In the presences of an external magnetic or electric field within a few milliseconds MR fluid can exchange to semi-solid state from free-flowing state and able to form chain-like fibrous structure (Kordonsky, 1993, Chen and Liao, 2010). MR dampers are mainly used in automobiles, civil construction such as buildings, bridges and frame structure, reducing floor vibrations, heavy motor damping, helicopter lag dampers, railway vehicles, and more (Ahmadian and Koo, 2003; Zhao *et al.*, 2004; Ahmadian and Sandu, 2008; Hu and Wereley, 2008; Wang and Liao, 2009; Bai and Wereley, 2014; McLaughlin *et al.*, 2014).

A big amount of vibration energy is vanished during the everyday use of an automobile under road irregularities, which is created by MR damper vibration. This unused vibration or mechanical energy can be used as a power

sources if this energy can be transferred into the electrical energy (Velinsky and White, 1980). Therefore, extra power supply would not be needed if this energy can be used as the MR damper power source and extra sensor would not be required, if the dynamic responses can be measured except an accessory sensor. This self-powered and self-sensing technology has no harmful effects of the environment and this technology will improve the credibility of whole MR damper systems. It has massive advantages for example, weight and size reduction, simpler way form, less maintenance cost and continuous controllability are very beneficial under some extreme condition such as earthquakes when the power supply may be cut off.

Some researches have been accomplished formerly on the power generation ability of the MR damper such as Cho *et al.* (2005) introduced an MR damper with power regeneration which has an electromagnetic induction device for reducing suspension vibrations. It gives a technological plan for self-powered vibration control and the electromagnetic induction (EMI) exploits vibration energy to produce electrical energy. Its size would be big that's why may not be applicable in small placing position, such as car, bus, motorcycles, and robots. Choi and Wereley *et al.* (2009) studied the liability and effectiveness of a self-powered MR damper and used a spring-mass electromagnetic induction device. The produced energy was used as the source of MR damper outright to escape the use of accessory sensors. Whereas, it is not proper for different applications because of the control algorithm is settled. Sapinski (2010) introduced a power generator for a linear MR damper which is known as an electromagnetic power generator. Mainly in this work the performance and construction design of the generator were focused. Moreover, Hu *et al.* (2014) designed a novel MR damper, having self-sensing ability. The proposed technology can give

\*Corresponding author; E-mail: raju.ahamed@live.iium.edu.my

<sup>†</sup>Co-corresponding author; E-mail: mahbub@iium.edu.my

controllable damping force and displacement relative self-induced voltages simultaneously but has no power generation ability. Sun *et al.* (2015) proposed a self-sensing technology for vibration absorber which has capability to allow the absorber to operate without sensors. At the same time, this technology can greatly reduce the maintenance costs and required space.

Furthermore, Chen and Liao (2012) first proposed a self-sensing self-powered MR damper by considering the previous mentioned development of MR dampers and filed for patent applications. It is only applicable for double ended MR dampers and civil structures. Ferdaus *et al.* (2013) proposed a self-powered MR damper where the permanent magnet generator is attached with piston head inside the MR damper. According to this, design the attachment of permanent magnet generator inside the MR damper on the piston head is a very complex system as well as costly. Bogdan Sapinski (2014) designed and tested an energy-harvesting linear prototype MR damper which has three main components in one device. The advantage of this model is that it does not need a power supply nor a sensor due to its self-powered and self-sensing capabilities. However, the disadvantages of this model are its limited output voltage and its weight.

With the aim of reducing the amount of electric power and to increase reliability of the MR damper, this paper is proposing a new design concept of power generation ability of the mono tube magnetizing device involving a hybridized magnetic field source by means of permanent magnet and electromagnet. It would be convenient to integrate the power generation and controllable damping tech-

nologies within one device.

## 2. Design Description of the Proposed Model

The proposed energy generated MR damper model has a damping part and an energy generation part. The energy generation part consists permanent magnet and coil. The magnet is attached to the outside wall of the damper body and the outside coil is attached to the piston rod as shown in Fig. 1. The non-magnetic material is attached between the place of the magnet and damper outside wall for minimizing the magnetic effect of the magnet. When the piston moves, the coil moves along with the piston rod and cuts the magnetic flux of the magnet and produced electrical power.

### 2.1. Magnetic field produced by permanent magnet and coil

The cylindrical-shaped permanent magnet of the proposed MR damper produces a magnetic field which can be described in the similar methodical design of a cylindrical-shaped copper coil (Ravaud *et al.*, 2011; Furlani *et al.*, 1995). Fig. 2 presents the design of the cylindrical per-

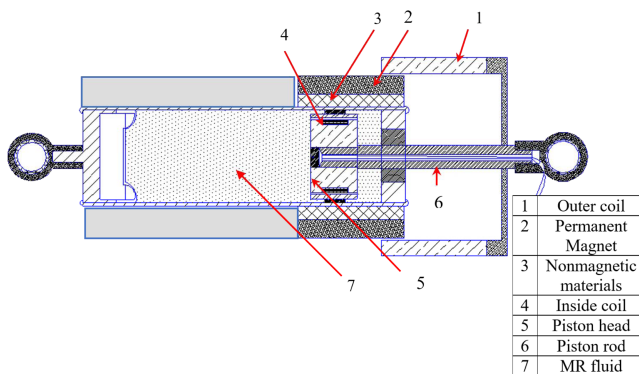


Fig. 1. (Color online) Energy generated MR damper model.

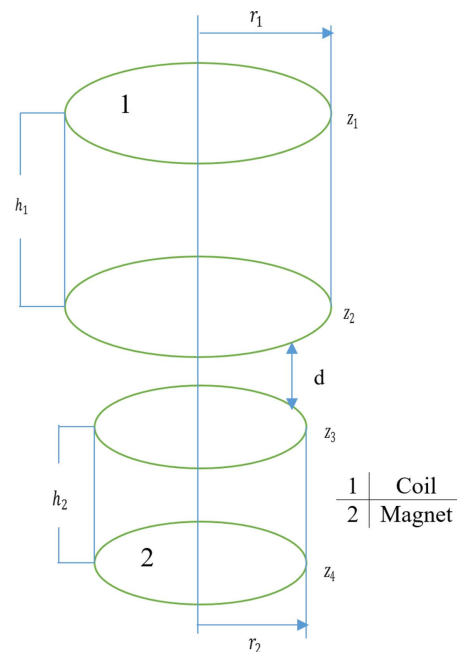


Fig. 2. (Color online) Magnet and coil arrangement.

Table 1. Parameters of the magnet and coil arrangement.

Symbol	Specification	Symbol	Specification
$J(T)$	Polarization of the permanent magnet	$r_1$	Radius of the coil
$N$	Number of turns of the coil	$r_2$	Radius of the magnet
$I(A)$	Current of the coil	$h_1 = z_2 - z_1$	Height of the coil
$d$	Axial distance between the magnet and coil	$h_2 = z_4 - z_3$	Height of the magnet



**Fig. 3.** (Color online) (a) Coil and (b) magnet for proposed energy generated MR damper.

manent magnet and the coil of the proposed MR damper model. All parameters of the Fig. 2 are shown in Table 1. Moreover, Fig. 3 shows the coil and magnet assembly for proposed energy generated MR damper model where Fig. 3a is coil and Fig. 3b is permanent magnet.

The current surface density of the coil is  $K$  which is equal to  $NI/h_1$ . The permanent magnet produces magnetic induction field which is expressed by using the Biot-Savart Law (Ravaud *et al.*, 2011).

$$\vec{B}(\vec{r}, \vec{z}) = \frac{\mu_0}{4\pi} \iint_S \vec{k} d\vec{s} \times \{-\nabla G(\vec{r}, \vec{r})\}. \quad (1)$$

In Eq. (1),  $\vec{B}$  is the magnetic induction field and  $G(\vec{r}, \vec{r})$  is the Green's function that is well-defined as Eq. (2).

$$G(\vec{r}, \vec{r}) = \frac{1}{\sqrt{\tilde{r}^2 + \tilde{r}^2 - 2\tilde{r}\tilde{z} \cos(\tilde{\theta}) + (\tilde{z} - \tilde{z})^2}}. \quad (2)$$

Moreover, the notation  $\tilde{r}$  is known as the parallel to the points positioned on the permanent magnet and  $\tilde{r}$  is known as corresponding points situated on the coil. It is found in Eqs. (3) and (4), the two magnetic induction field component  $B_r(r, Z)$  and  $B_z(r, Z)$  after integrating  $\tilde{r}$  and  $\tilde{z}$ .

$$B_r(r, Z) = \frac{(\mu_0 k)}{2\pi} C_a = \frac{(\mu_0 NI)}{2\pi h_1} C_a, \quad (3)$$

$$B_z(r, Z) = \frac{(\mu_0 k)}{2\pi} C_b = \frac{(\mu_0 NI)}{2\pi h_1} C_b, \quad (4)$$

where  $C_a$  and  $C_b$  are known as scalar coefficients that confide on the foundation topology;

$$C_a = \sum_{i=1}^2 (-1)^i \left\{ \frac{a_i}{r\sqrt{\alpha_i}} K \left[ \frac{-2b}{\alpha_i} \right] - \frac{\sqrt{\alpha_i}}{r} E \left[ \frac{-2b}{\alpha_i} \right] \right\}, \quad (5)$$

$$C_b = \sum_{i=1}^2 (-1)^i \varepsilon_{4,i} \{ (cr - br_1) (\Pi[\varepsilon_{1,i}, \varepsilon_{3,i} \varepsilon_{2,i}] + \Pi[\varepsilon_{1,i}, \varepsilon_{2,i}]) + (b_{r1} - a_i r) (F[\varepsilon_{3,i}, \varepsilon_{2,i}] + K[\varepsilon_{2,i}]) \}. \quad (6)$$

In Fig. 2 the axial polarization of the permanent magnet is  $J$ . The magnetic induction field produced by the permanent magnet can be stated by Eqs. (7) and (8).

$$B_r(r, z) = \frac{J}{2\pi} C_a, \quad (7)$$

$$B_z(r, z) = \frac{J}{2\pi} C_b. \quad (8)$$

## 2.2. Analysis of energy generation

The electromagnetic transduction mechanism is used here to essence energy. The power produced system includes magnet and coil assemblies. The outer assembly consists coil and inner assembly consists magnet and non-magnet. If the piston rod is allowed to move, then the coil will move along the magnet axis, an electric field will develop in the coil such as to oppose the magnet's motion. This field produces an electric potential  $V$  across the coil's leads, which Faraday's law of induction predicts to be proportional to the time rate of change in magnetic flux through the coil (Furlani, 2001). Avoiding eddy current losses, the induced voltage can be stated as Eq. (9).

$$V = - \frac{d}{dt} \oint_S B \cdot da = - \dot{\Phi}_{tot} \quad (9)$$

where the produced potential voltage in the coil is  $V$ ,  $S$  is a surface that encloses the conductor and  $da$  is an area element normal to  $S$ . Moreover,  $\dot{\Phi}_{tot}$  is the magnetic flux through the coil and an over dot indicates a time derivative. By insulating the  $n$ th turn of the coil and considering it as a single turn coil, above equation can be rewritten by Eq. (10).

$$V_n^{(1)} = - \frac{d}{dt} \oint_{S_n} B \cdot da = - \dot{\Phi}_n^{(1)} \quad (10)$$

where  $S_n$  is the enclosing surface, superscript (1) indicates the single turn coil, and  $V_n^{(1)}$  is the induced voltage. Furthermore,  $\dot{\Phi}_n^{(1)}$  is magnetic flux allied with the coil (single turn). The equation can be expressed by Eq. (11).

$$V = \lambda y \sum_{n=1}^N \frac{\tilde{r}_n^2 (\hat{x}_n - y)}{(\tilde{r}_n^2 + (\hat{x}_n - y)^2)^{5/2}} \frac{A_{wn}}{\Delta A_n}. \quad (11)$$

The total magnetic flux through the coil is thus

$$\Phi_{tot} = \sum_{n=1}^N \Phi_n, \quad (12)$$

$$\Phi_n = \Phi_n^{(1)} A_{wn} / \Delta A_n, \quad (12a)$$

$$\Phi_n^{(1)} = \frac{1}{A_{wn}} \int_{A_{wn}} \left( \int_0^{2\pi} \int_0^r B(\tilde{r}, x, y) \cdot \hat{e}_x \tilde{r} d\tilde{r} d\varphi \right) dA, \quad (12b)$$

$$\Phi_n^{(1)} = \frac{1}{A_{wn}} \int_{A_{wn}} -\frac{1}{3} \lambda r^2 [r^2 + (x-y)^2]^{-3/2} dA, \quad (12c)$$

$$\Phi_n^{(1)} \approx -\frac{1}{3} \lambda \tilde{r}_n^2 [\tilde{r}_n^2 + (\hat{x}_n - y)^2]^{-3/2} \quad (12d)$$

where  $A_c$  is cross-sectional area of the coils and  $A_{wn}$  is the wire area. Moreover,  $dA$  is an infinitesimal area element within the wire cross-section,  $\varphi$  is a polar angle coordinate, and  $\tilde{r}$  is a dummy radial coordinate.

## 2.3. Damping force of the proposed MR damper

In order to model the nonlinear performance of the MR

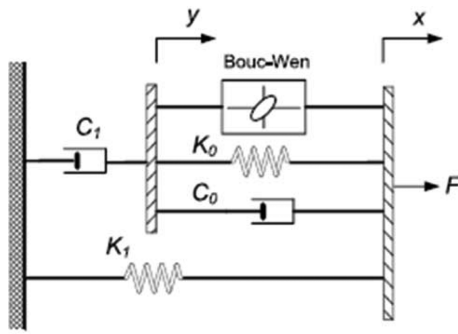


Fig. 4. The modified Bouc-Wen model of the MR damper.

damper, the improved Bouc-Wen model, shown in Fig. 4, is applied in this study. The proposed model consists mechanical springs and energy generated damper, along with a hysteresis element. The modified Bouc-Wen model has been shown to accurately predict the nonlinear behavior of prototype MR dampers over a wide range of operating conditions (Spencer Jr. *et al.*, 1997).

In the improved Bouc-Wen model, the damping force of the MR damper is given by

$$F = C_1 \dot{y} + K_1(x - x_0) \quad (13)$$

where the velocity  $\dot{y}$  is given by

$$C_1 \dot{y} = \alpha z + K_0(x - y) + C_0(\dot{x} - \dot{y}) \quad (14)$$

where  $z$  is the hysteretic displacement, whose spread equation is

$$\dot{z} = -\gamma |\dot{x} - \dot{y}| |z|^{n-1} - \beta (\dot{x} - \dot{y}) |z|^n + A(\dot{x} - \dot{y}) \quad (14a)$$

with the parameters  $\gamma$ ,  $\beta$ ,  $A$ , and  $n$  governing the character of the hysteresis loop. Since, in a MR damper, the rheological properties of its fluid may be reversibly changed by exposing it to a controlled magnetic field, some parameters of the model are assumed to be dependent on the voltage  $V$  applied to the current driver as follows:

$$\alpha = \alpha(I) = \alpha_a + \alpha_b(I), \quad (14b)$$

$$C_1 = C_1(I) = c_{1a} + c_{1b}I, \quad (14c)$$

$$C_0 = C_0(I) = c_{0a} + c_{0b}I \quad (14d)$$

where the internal variable  $I$  is the output of the first order filter that accounts for the dynamics involved in reaching the rheological equilibrium (Spencer Jr. *et al.*, 1997), viz.  $C_1$  and  $C_0$  are suspension damping coefficient.

### 3. Finite Element Analysis and Characterization of Proposed MR Damper Model by EMS

The permanent magnet is attached in the outside body of the damper which has possibility to create magnetic interaction with damper MR fluid. To minimize the magnetic interaction issue from damper body and damper MR fluid

Table 2. Parameter selection.

Parameter	Value
Piston head coil turn	400
Outer coil turn	200
Magnet thickness	8 mm
Coil thickness	6 mm
Resistance of the outer coil	2.6 $\Omega$
Outer coil wire diameter	0.6 mm
Diameter of the outer coil	98 mm
Diameter of the permanent magnet	88 mm
Applied current	0.5 A
Piston head diameter	38 mm
Air gap (between coil and magnet)	4 mm

Table 3. Material selection.

Parameter	Selected materials
Piston head	Iron
Piston rod	Steel
Damper body	Carbon iron
Coil	Copper
Permanent magnet	Grade 6 (NdFeB)
Nonmagnetic material	Plastic

the finite element analysis has been simulated. EMS (Electromagnetic simulation) software has been chosen for fine element analysis. EMS is a 3D electromagnetic field simulator software and it is Add-in to Solid Works. Magneto static module has been selected to study the magnet interaction issue of the proposed model. All boundary conditions have been adopted from the toolbox as shown in Table 2. Permanent magnet, coil and another materials have been selected from materials library as listed in Table 3. Coil types, coil turn number, coil resistant, and coil area size have been decided from coil selection tool bar. After meshing, the finite element analysis is shown in Fig. 5. Fig. 6 presents the cross sectional view of damper magnetic density. The current applied inside the damper piston head than the piston head coil produced magnetic field around the piston head as shown in Fig. 6a. In Fig. 6b, the magnetic flux density value is actually represented in tesla. For 0.5 (A) current the flux density varies from 0 to 1.28 Tesla in the damper body. The color presents the variations of magnetic flux density. Observing closely is obvious that higher flux density is produced around the piston head coil area and the permanent magnet area which are expressed by the color variation.

For clearer inspection, the magnetic flux density is illustrated in Fig. 7. It is seen from the Fig. 7 that the magnetic field spreads inside the outer coil. The magnetic field intensity has higher value around permanent magnet and piston head coil area. But, around damper body area its

Design and modeling of energy generated magneto rheological damper

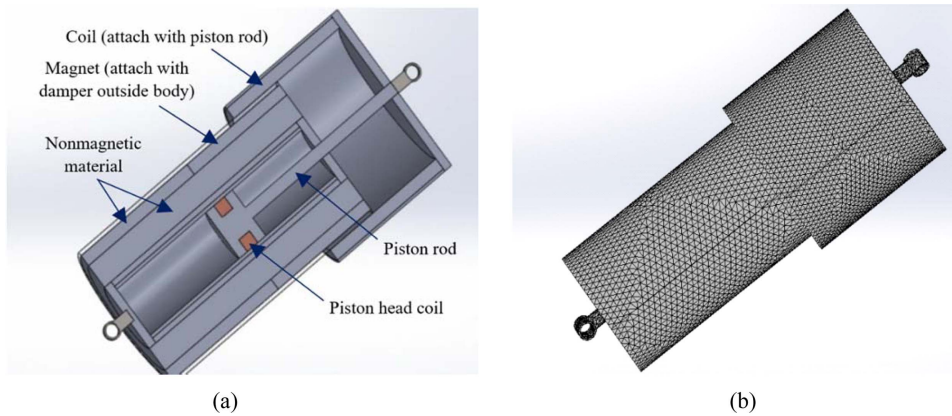


Fig. 5. (Color online) (a) Solid Works Cross-sectional view before meshing and (b) Mesh configuration of energy generated MR damper.

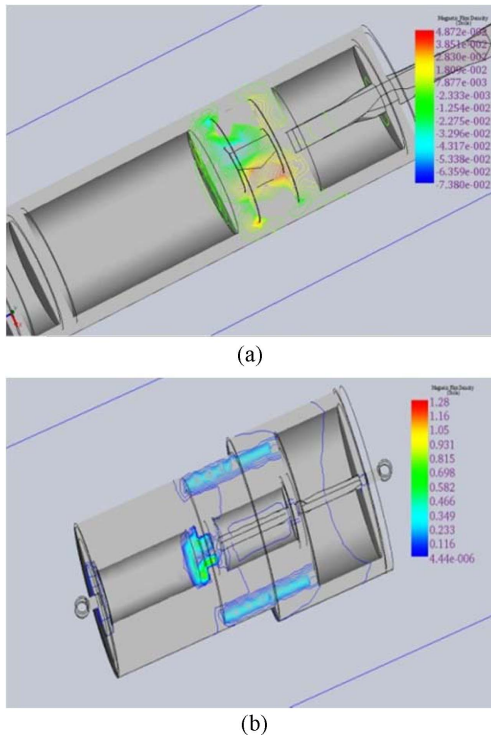


Fig. 6. (Color online) Cross-sectional clipping view of magnetic flux density (contour fringe view): (a) Damping part and (b) damping and energy generation parts.

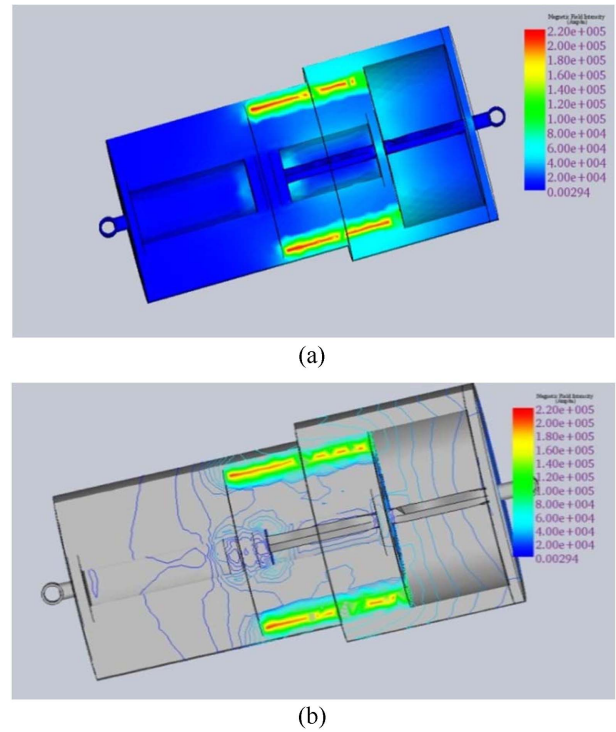
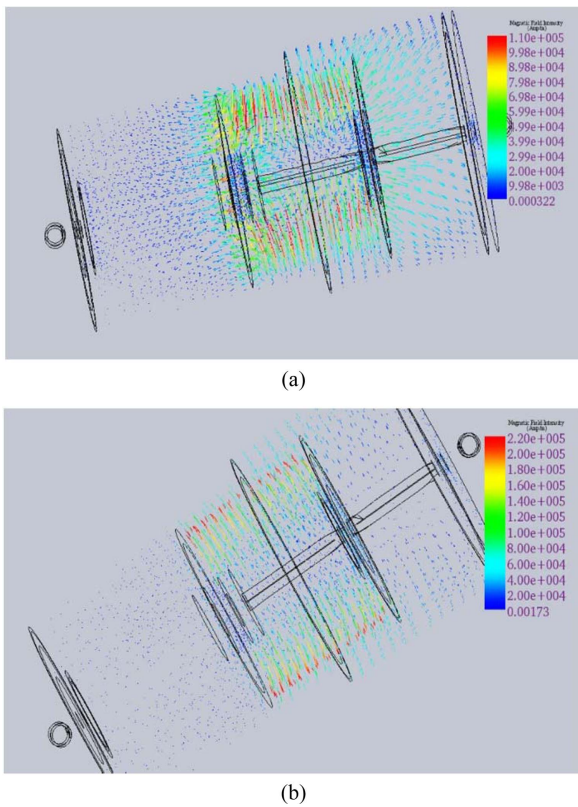


Fig. 7. (Color online) Cross-sectional view of magnetic field intensity of the model: (a) Fringe contour and (b) fringe line.

value almost zero. It can be said from this observation that the attached permanent magnet has no magnetic interaction problem. The magnetic field intensity produced by the permanent magnet and the coils is analyzed by finite element vector plotting by ignoring axis correspondingly as exposed in Fig. 8. The magnetic field intensity is not same among two figures, that is, the magnetic field intensity is different at the two different axes.

Fig. 8a has shown magnetic field intensity produced by the coils. In Fig. 8b, the color variations represent the magnetic field intensity of the model which actually

expresses the intensity of magnetic field around the permanent magnet and the outside coil. Moreover, the outer coil is moving along with piston rod, so this moving coil cuts the magnetic field of the magnet, producing the induced magnetic flux inside the coil as presented Fig. 8. According to Faraday's law, voltage is induced in the outer coils. These outer coils connect to the inner coils and these induced voltages of the outer coils are being used as loads to the inner coils. This close path creates opportunity to outer coils for supplying current to the inner coils where the amount of current depends upon the frequency of the piston rod movement.



**Fig. 8.** (Color online) Magnetic flux density of MR damper model vector plotting: (a) X vector plotting and (b) Y vector plotting.

#### 4. Experimental Results and Discussion

The experimental setup consists an MR damper, a current controller, and a universal testing machine (UTM) of Instron, as displayed in Fig. 9. The UTM is used to test and analyze the MR damper and the input excitation from the UTM is staircase steps. The upper end is the movable head and it is operated by a hydraulic actuator which takes Instron bluehill software signal generated from the computer. In this experiment, the damping characteristics and voltage generation from damper have been analyzed. Fig. 10 shows the relation between the damping force and stroke length.

As established in Fig. 10, when the current is zero, the force vs stroke graph is almost constant at different stroke lengths. For the same stroke rate, the peak force is obtained at 0.8 A, which is higher than the force at other current values. As the supply current to the MR damper increases, the peak value of the graph rises correspondingly. That implies that the ruffian vibratory vitality increases with the rising current values. It is additionally seen from Fig. 10, that the damping force increases from 55 to 450 N when the DC current is expanded from 0 to 0.8 A. This phenomenon is more obvious in Fig. 11, which exhibits the force and applied current relationship for different stroke lengths.

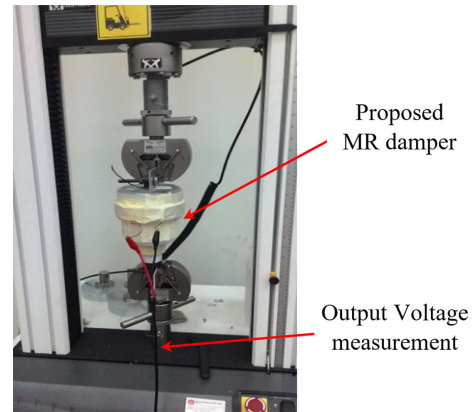


**Fig. 9.** (Color online) Experimental setup of the proposed MR damper with UTM.

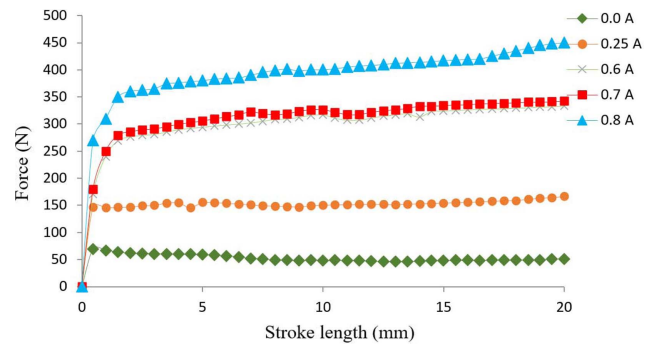


**Fig. 10.** (Color online) Force and damper stroke length relations of the MR damper with different applied current under 100 mm/min velocity, 20 mm displacement.

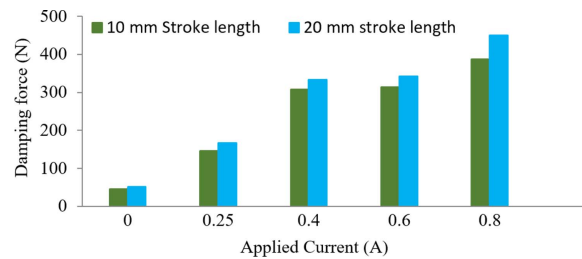


**Fig. 11.** (Color online) Relation between damping force and applied current.

From Fig. 11, it can be concluded that, the damping force has relation to the damping stroke length. For the same current, the damping force increases with the increase of stroke length. For 0 A current and stroke length of 10 mm the damping force is calculated about 45 N, whereas for 20 mm stroke length, nearly 51 N is obtained for the same excitation current. Similarly, for 0.8 A applied current, this damping force for 20 mm stroke length is higher than that of 10 mm stroke length. Fig. 12 shows the relation between damping force and time.

From Fig. 12, it is clear that the damping force increases with the increase of the applied current as well as damping

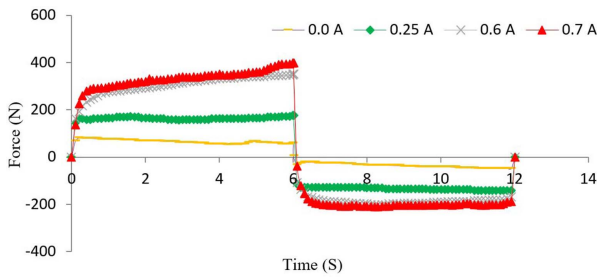


**Fig. 12.** (Color online) Force vs. time relations of the MR damper with different applied currents under 100 mm/min velocity and 20 mm displacement.

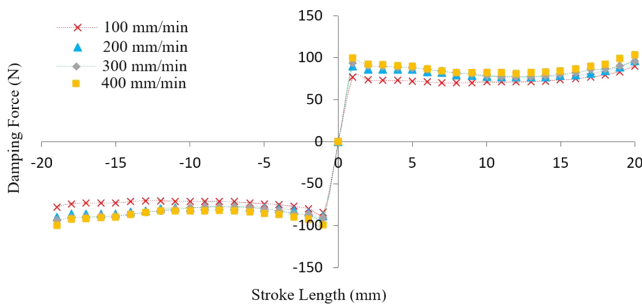
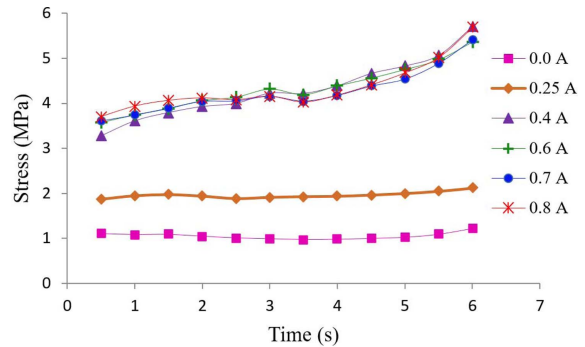


**Fig. 13.** (Color online) Relation between damping force and velocity.

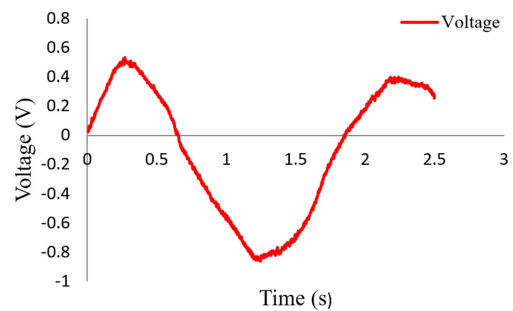
time. It is also seen from Fig. 12 that the damping force increases from 50 to 400 N when the time is expanded from 0 to 6 s. The piston forward moving damping force is higher than the piston backward moving damping force as seen in Fig. 12. Fig. 13 presents the damping force and damping velocity relation for 0 A applied current and 20 mm damping stroke length.

Fig. 13 exposes that the damping force increases with the increasing velocity of the piston. For 100 mm/min velocity, the peak damping force is about 70 N, which touches to 100 N for 400 mm/min velocity. The compressive stress has relation to time and applied current as displayed in Fig. 14. From Fig. 14, it can be summarized that, the stress increases with the increasing of damping time and applied current. When the applied current is 0 A, then the maximum stress is around 1 MPa and this stress increases with the increase of applied current which has shown by color variation. The red color shows the maximum stress for maximum applied current (0.8 A). When the UTM machine moves linearly, then the piston rod moves with UTM upper end. The coil also moves with piston rod and cuts magnetic field of the permanent magnet. The generated voltage as shown in Fig. 15 is measured by Oscilloscope. Fig. 16 shows the relation of generated voltage with stroke length and velocity.

It can be said from Fig. 16 that the induced voltage increases with the increase of excitation and velocity. For 20 mm excitation, the induced voltage reaches about 0.8 volts with increasing velocity, which is higher than the



**Fig. 14.** (Color online) Relation between stress and applied current in MR damper.



**Fig. 15.** (Color online) Induced voltage of the coil.

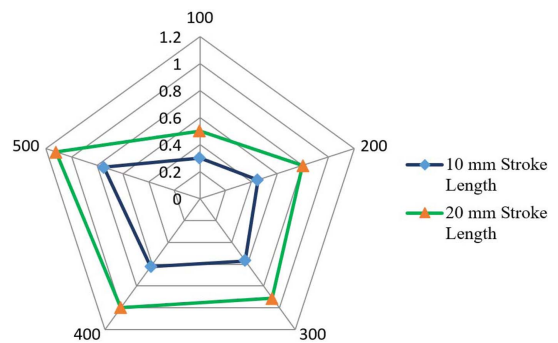


**Fig. 16.** (Color online) Induced voltage of the coil under 20 mm stroke with various stroke velocities.

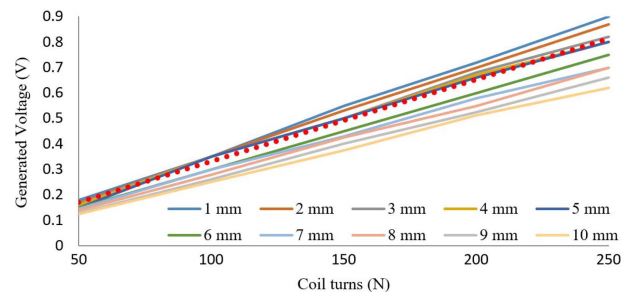


**Fig. 17.** (Color online) Relation among the coil turn numbers, air gaps, and induced voltage.

case by 10 mm excitation. Fig. 17 displays the relation of generated voltage with coil turn number and air gap. From Fig. 17, it is clear that the induced voltage increases with

increasing the coil numbers, but decreases with increasing the air gap. The dotted red line presents the optimized air gap for the model. The induced voltage decreases with increasing the air gap but for these three (3 to 5 mm) air gaps, the induced voltage is almost same. This is a great achievement of this work due to the successful magnetic field isolation between closely situated two magnetic sources.

## 5. Conclusions

Advancement in MR damper technology is one of the challenging researches in the vibration control area. Making the damper self-powered is a recent advancement, but it is accomplished for only twin tube MR damper. In this study, a mono tube MR damper model is developed, which has power generation ability. Here solid works EMS based finite element analysis is accomplished for characterizing and validating the model's accuracy of minimizing magnet interaction issue. In this damper model, permanent magnets and coils are used as power generator that utilizes wasted vibration energy from the vehicle. From experimental study, the power generation feature and all the results are clearly validating that quality. The magnetic isolation between two separated fields has been clearly observed from those results. So it can be concluded that the developed mono tube MR damper model works effectively as self-powered device.

## Acknowledgements

The authors would like to thank the Department of Mechatronics Engineering, International Islamic University for giving the opportunity of use the Vibration and Smart Materials Laboratory and Ministry of Higher Education Malaysia for funding the project FRGS/1/2014/TK03/UIAM/02/4.

## References

Ahmadian, M. and J.H. Koo, 2003, On the application of magneto-rheological dampers for reducing floor vibrations, *J. Acoust. Soc. Am.* **114**, 2385-2385.

Ahmadian, M. and C. Sandu, 2008, An experimental evaluation of magneto-rheological front fork suspensions for motorcycle applications, *Int. J. Veh. Syst. Model. Test.* **3**, 296-311.

Bai, X.-X. and N.M. Wereley, 2014, A fail-safe magnetorheological energy absorber for shock and vibration isolation, *J. Appl. Phys.* **115**, 17B535.

Chen, C. and W.-H. Liao, 2012, A self-sensing magnetorheological damper with power generation, *Smart Mater. Struct.* **21**, 025014.

Chen, J. and W.-H. Liao, 2010, Design, testing and control of a magnetorheological actuator for assistive knee braces, *Smart Mater. Struct.* **19**, 035029.

Cho, S.-W., H.-J. Jung, and I.-W. Lee, 2005, Smart passive system based on magnetorheological damper, *Smart Mater. Struct.*

**14**, 707-714.

Choi, Y.-T. and N.M. Wereley, 2009, Self-powered magnetorheological dampers, *J. Vib. Acoust.* **131**, 044501.

Ferdaus, M.M., M.M. Rashid, M. Bhuiyan, A.G.B.A. Muthalif, and M. Hasan, 2013, Novel design of a self powered and self sensing magneto-rheological damper, *IOP Conf. Series: Mater. Sci. Eng.* **53**, 012048.

Furlani, E., S. Reznik, and A. Kroll, 1995, A three-dimensional field solution for radially polarized cylinders, *IEEE Trans. Magn.* **31**, 844-851.

Furlani, E.P., 2001, *Permanent Magnet and Electromechanical Devices: Materials, Analysis, and Applications*, Academic Press.

Gattulli, V., M. Lepidi, F. Potenza, and R. Carneiro, 2008, Semi-active control using MR dampers of a frame structure under seismic excitation, *AIP Conf. Proc.* **1020**, 153-161.

Hu, G., Y. Ru, and W. Li, 2014, Design and development of a novel displacement differential self-induced magnetorheological damper, *J. Intel. Mater. Syst. Struct.*, 1045389X14533429.

Hu, W. and N.M. Wereley, 2008, Hybrid magnetorheological fluid-elastomeric lag dampers for helicopter stability augmentation, *Smart Mater. Struct.* **17**, 045021.

Karnopp, D., M.J. Crosby, and R. Harwood, 1974, Vibration control using semi-active force generators, *J. Manuf. Sci. Eng.* **96**, 619-626.

Kordonsky, W., 1993, Elements and devices based on magnetorheological effect, *J. Intel. Mater. Syst. Struct.* **4**, 65-69.

Lai, C.Y. and W.-H. Liao, 2002, Vibration control of a suspension system via a magnetorheological fluid damper, *J. Vib. Control* **8**, 527-547.

Mclaughlin, G., W. Hu, and N. Wereley, 2014, Advanced magnetorheological damper with a spiral channel bypass valve, *J. Appl. Phys.* **115**, 17B532.

Ravaud, R., G. Lemarquand, and V. Lemarquand, 2011, Coils and magnets: 3D analytical models, *PIERS Proc.*, Morocco, 1178-1184.

Sapiński, B., 2010, Vibration power generator for a linear MR damper, *Smart Mater. Struct.* **19**, 105012.

Sapiński, B., 2014, Energy-harvesting linear MR damper: prototyping and testing, *Smart Mater. Struct.* **23**, 035021.

Shen, Y., M. Golnaraghi, and G. Heppler, 2006, Semi-active vibration control schemes for suspension systems using magnetorheological dampers, *J. Vib. Control* **12**, 3-24.

Spencer Jr., B., S. Dyke, M. Sain, and J. Carlson, 1997, Phenomenological model for magnetorheological dampers, *J. Eng. Mech.* **123**, 230-238.

Sun, S., J. Yang, W. Li, H. Deng, H. Du, and G. Alici, 2015, Development of an MRE adaptive tuned vibration absorber with self-sensing capability, *Smart Mater. Struct.* **24**, 095012.

Velinsky, S.A. and R.A. White, 1980, Vehicle energy dissipation due to road roughness, *Vehicle Syst. Dyn.* **9**, 359-384.

Wang, D. and W. Liao, 2009, Semi-active suspension systems for railway vehicles using magnetorheological dampers. Part I: System integration and modelling, *Vehicle Syst. Dyn.* **47**, 1305-1325.

Zhao, Y., Y.T. Choi, and N.M. Wereley, 2004, semi-active damping of ground resonance in helicopters using magnetorheological dampers. *J. Am. Helicopter Soc.* **49**, 468-482.